Sl. No.	IIT Ropar List of Recent Publications with Abstract Coverage: September, 2024
A	**Book Chapter(s)**
1.	Agro-forestry biomass as a potential bioresource for climate change mitigation **A Jaswal, PP Singh**, S Lande, **T Mondal** - Clean Energy Transition-via-Biomass Resource Utilization: A Way to Mitigate Climate Change: Book Chapter, 2024 **Abstract:** Energy demand and the evolutionary trajectory of human civilization are fundamentally intertwined. The discovery and exploitation of emerging energy technologies have been instrumental in driving exceptional progress, both socio-culturally and economically, across historical epochs.
2.	Properties of 2D semiconducting materials **SP Kaur, TJ Dhilip Kumar** - 2D Semiconducting Materials for Electronic, Photonic, and Optoelectronic Devicces: Book Chapter, 2024 **Abstract:** The chapter delivers the outline of the varied range of properties of two-dimensional semiconducting materials (2D-SCMs) in various sectors. The chapter introduces a brief introduction of the structure of 2D-SCM monolayer, bilayer, or heterostructures, highlighting the unique properties. Subsequently, the optical properties of 2D-SCMs are reviewed, including modulation of bandgap engineering, photoluminescence, absorption spectra, and their tuning to external pressure or applied strain. The electrical properties of 2D-SCMs are thoroughly examined in terms of electronic bandgap, carrier transport mechanisms, and so on. Thermal properties of 2D-SCMs are examined, focusing on thermal conductivity, phonon transport, and their relevance in thermoelectric applications. Moreover, the mechanical properties of 2D-SCMs are highlighted, encompassing their mechanical behavior, flexibility, and the impact of strain engineering. The chapter concludes by summarizing the key points and underlining the importance of understanding the properties of 2D-SCMs. The associated challenges such as stability and future directions to leverage the full potential of 2D-SCMs are also discussed.
3.	Strategies and implementation for achieving sustainable flood risk **NG Paswan, S Pathak** - Sustainable Development and Geospatial Technology: Volume 2: Applications and Future Directions: Book Chapter, 2024 **Abstract:** Flood is considered one of the most destructive and catastrophic phenomena among all-natural calamities. Flood risk is a function and a product of hazard and vulnerability. The selection of appropriate flood management strategies necessitates a thorough understanding of the risk mechanism. Flood Risk Management (FRM) approaches are critical for reducing the devastating effects floods can have on human health, economy and the environment. FRM comprises a variety of tactics and approaches for mitigating these impacts, whether on a local or a global basis. FRM employs a systematic strategy that has proven critical for mitigating flood-related risks. This chapter examines various FRM approaches, analysing their limitations, characteristics and key components. Furthermore, the chapter discusses the importance of remote sensing and Geographic Information Systems (GISs) in supporting FRM activities. Using these tools, stakeholders, urban planners and watershed managers can better forecast and minimise the effects of floods through proactive actions.
B	**Conference Proceeding(s)**

4.	A fault-tolerant single-phase inverter using redundant leg **A Tripathi, PS Bhakar, J Kalaiselvi** - 2024 IEEE International Communications Energy Conference (INTELEC), 2024 **Abstract:** Single-phase inverters are increasingly used in a variety of applications from renewable energy systems to un-interruptible power supply. In the design and operation of these inverters, reliability remains a major concern. The single-phase inverter offers fault tolerance by including a redundant leg. The conventional redundant leg configuration uses four triode for alternating current (TRIAC) and two switches. The voltage seen across TRIACs used to connect the redundant leg is pulse width modulated (PWM). The high dv/dt across the TRIACs in the conventional topology due to PWM causes spurious turn ON across TRIACs. It leads to a short-circuit (SC) across the terminals. Thus, there is a need to modify the conventional TRIAC arrangement that is used to connect the redundant leg. In this paper, an updated TRIAC arrangement for a fault-tolerant single-phase inverter is proposed. The proposed TRIAC arrangement uses a split inductor filter to provide a sinusoidal voltage across the TRIACs. Thus the rearrangement of TRIAC ensures the lower dv/dt across the terminals. The reconfiguration of TRIACs is verified in simulation and experimentally through a 200V single-phase inverter with redundant leg prototype.
5.	AeroDehazeNet: Exploiting selective multi-scale transformers for aerial image dehazing K Gonde, PW Patil, **SK Vipparthi**, S Murala, P Patil, V Kimbahune - 2024 IEEE International Conference on Advanced Video and Signal Based Surveillance (AVSS), 2024 **Abstract:** Remote sensing is the task of analyzing and acquiring useful information from satellite images captured at a far distance from the earth's surface. These images are vulnerable to degradation due to the presence of mist or haze. Existing methods either make use of prior information to estimate haze free images, or use CNN architectures based on generative adversarial networks (GANs) or Transformers. Though the state-of-the-art transformer-based architectures helped to dehaze the aerial images, they lacked the ability to capture multi-scale dependencies of the image. Identifying this shortcoming, we propose AeroDehazeNet based on a transformer that captures multi-scale dependencies along with global dependencies of the image. Our network comprises of three key components: (1) a multi-scale selective attention (MScA) network to attentively process the multi-scale information in an image, (2) residual attention network (RAN in feed forward network responsible for distilling non-degraded features passed from MScA, and (3) high frequency dominant skip connection (HFDS) block for passing diverse features (low frequency and high frequency) prominent with multi-scale edge features from encoder levels to adjacent decoder levels. The extensive quantitative and qualitative comparisons with existing methods on synthetic and realworld data plus exhaustive ablation study demonstrate the efficacy of our proposed network over transformer based state-of-the-art architectures with comparatively less number of parameters and FLOPs. Testing code is available at https://github.com/KartikGonde/AeroDehazeNet.
6.	Burnsnet: Burn region segmentation network from color images with two-way CNN **J Chauhan**, PL Rosin, **P Goyal** - 2024 IEEE International Conference on Image Processing (ICIP), 2024 **Abstract:** Burn injury is a serious health issue leading to several thousands of annual fatalities. The color image-based automated burns diagnostic and assessment methods hold the potential for timely diagnosis and treatment. However, the research is limited in this domain which remains a major challenge. In this work, we explore and address the complex task of burn region segmentation in color images of burn patients. We present a semantic segmentation network that has two parallel sub-networks: a spatial-stream network for extracting low-level features and a contextual-stream network for generating a larger receptive field. Our network utilizes the pre-trained ResNet101 network, global average pooling, and instance normalization for better

	encoding and fusion of the network outputs. This dual-stream approach optimizes the performance in situations where data scarcity poses a challenge, facilitating robust semantic segmentation despite limited training samples. We prepared a pixel-wise labeled dataset for burn region segmentation and the experimental results on this dataset show that our proposed network outperforms several state-of-the-art semantic segmentation methods. Our method achieved mIOU and Matthews' correlation coefficient (MCC) of 74.3% and 81.7%, respectively, approximately 4.5% higher than the second-best performing method. The Extended Burn Image Segmentation (EBIS) dataset and our model are available at https://github.com/VEDAs-Lab/EBIS.
7.	Cache line pinning for mitigating row hammer attack P M, M Mutyam, **VK Tavva** - 53rd International Conference on Parallel Processing, 2024 **Abstract:** RowHammer attack is a serious security threat to DRAM-based memory that causes bit flips in nearby rows when a DRAM row is accessed frequently. Many mitigation strategies are proposed against the RowHammer attack, and a few of the mitigation strategies are adopted and implemented by the hardware vendors. But even the latest generations of DRAM-based memory with in-DRAM mitigation are found vulnerable to the RowHammer attack. We propose Cache Line Pinning (CLP) as a mitigation strategy against the RowHammer attack. CLP pins the blocks in the cache when it identifies a RowHammer activity on the DRAM row where the block resides. In-depth experimental analysis shows that, with CLP the performance is improved not just in the case of attack programs, but also for benign applications. With a thorough analysis of various design parameters and implementation overhead, we find CLP to be a highly ease-of-use approach resilient to even complex attack patterns.
8.	Demonstration of machine learning based receiver for miso system using software-defined radios **A Ahmad, S Agarwal** - 2024 IEEE International Conference on Machine Learning for Communication and Networking (ICMLCN), 2024 **Abstract:** Multi-antenna transmission plays a pivotal role in 5G-New Radio (5G-NR). The latest communication systems, including cellular networks and WiFi access points, consist of multiple transmitting antennas. These antennas collectively transmit shared information to the designated receiver, necessitating the use of sophisticated receivers. We present a machine learning (ML) based radio receiver implementation for a fully wireless Multiple-input–single-output (MISO) communication system using software-defined radios (SDR). MISO system results in significant improvements in received signal gain as the number of antennas increases. However, perfect channel state information (CSI) is required at the transmitter for signal precoding to achieve optimal performance. Here, we designed an ML-based radio receiver that can demodulate signals without any need for CSI. In this study, we showcase our recent implementation of the MISO system on a standard open-source SDR platform, where two antennas send signals that may combine constructively or destructively at the receiver due to varying channels, and an ML-based radio receiver successfully demodulates the combined signal. Also, we validate the results in terms of bit-error rate.
9.	Linear spectral mixing based super-resolution mapping of the SCATSAT-1 in snow cover analysis **V Sood, RK Tiwari**, S Singh - IGARSS 2024 - 2024 IEEE International Geoscience and Remote Sensing Symposium (IGARSS), 2024 **Abstract:** Indian Space Research Organization (ISRO) launched its all-weather satellite on September 26, 2016 named as Scatterometer Satellite (SCATSAT-1). It is single band satellite operating at 13.5 GHz frequency. SCATSAT-1 is having the wide application range like ocean exploration, land hydrology, vegetation and cryosphere applications. Many fields like forecasting of weather, early prediction of the cyclones, snow hydrology studies, variations in sea-ice, Crop monitoring etc have become easy to investigate with the help of SCATSAT-1. SCATSAT-1 have advantages over other satellites like day and night operational, cloud penetration, global

	coverage, daily data availability, and extensive application area. In this work the Uttarakhand area has been explored. The SCATSAT-1 level-4 (L4) product and Moderate Resolution Imaging Spectroradiometer (MODIS) data have been considered for application of Super Resolution Mapping technique (SRM) to generate enhanced resolution results. The results of this study comply with enhancing the accuracy of classified maps using fusion technique as compared to any individual technique itself. The results have been validated using a reference dataset. This study offers cloud-free remote monitoring in all weather conditions using low resolution (LR) SCATSAT-1 data. Such exploration can be utilised in numerous areas like natural disasters, early snow-melt detection, and flood prediction.
10.	Non-coherent distributed transmission with chirp spread spectrum modulation **A Gupta, S Agarwal**, S Chakravarty - 2024 IEEE International Conference on Communications Workshops (ICC Workshops), 2024 **Abstract:** Efficient communication for internet-of-things (IoT) devices in remote rural areas, where resources are limited, remains a significant challenge. A communication technique capable of long-range, low-power communication is essential. Chirp spread spectrum (CSS) combined with multi-antenna transmission could be a potential solution. However, it's challenging to implement a multiple-input multiple-output (MIMO) configuration in small nodes. In this paper, we delve into the concept of distributed transmission using CSS waveforms to achieve extended communication range while maintaining the same transmit power. Achieving perfect synchronization among transmitters is intricate and time-consuming. Therefore, we resort to non-coherent distributed transmission (NCDT). In the presence of asynchronous transmitters, symbol detection is carried out using a least square (LS) detector. Simulation results demonstrate the better performance of the proposed NCDT-CSS in terms of bit error rate (BER), making it an efficient solution with less power usage for IoT devices in rural communication.
11.	Reconstruction of flood event occurred in Teesta Basin, Sikkim State, Eastern Himalaya: Combining hydrodynamical and hydrological modelling **D Gaikwad, VS Jadoun, RK Tiwari** - IGARSS 2024 - 2024 IEEE International Geoscience and Remote Sensing Symposium (IGARSS), 2024 **Abstract:** On October 4, 2023, a catastrophic Glacial Lake Outburst Flood (GLOF) originated from South Lhonak Lake (SLL) during a period of heavy rainfall in the Teesta basin, Sikkim Himalaya, resulting in widespread devastation and significant loss of lives. Therefore, this study intended to conduct the reconstruction of this flood event through an integrative approach, combining rainfall-generated runoff simulation and GLOF modelling using the Hydrologic Engineering Center - Hydrologic Modeling System (HEC-HMS) and Hydrologic Engineering Center - River Analysis System (HEC-RAS), respectively. The peak discharge estimated at Singtam from the HEC-HMS simulation, reflecting solely the rainfall effect, was 2409 m^3/s. In this contrast, the HEC-RAS modelling, which encompasses both rainfalls-induced runoff and GLOF from SLL, reveals a peak discharge of 6562.95 m^3/s. The results were optimised and validated by the flood parameter information of some active gauge sites of Central Water Commission (CWC) falls on the flood path. In summary, such studies improve the understanding by estimating and analysing the quantitative parameters of these events that occur during intense precipitation and sudden breaches of glacial lakes, coincidingly, which often occur in high mountain regions.
12.	Zero reference based low-light enhancement with wavelet optimization V Deshmukh, A Dukre, **A Kulkarni**, PW Patil, **SK Vipparthi**… - IEEE Conference on Advanced Video and Signal Based Surveillance (AVSS), 2024 **Abstract:** Images captured in low light conditions usually suffer from poor visibility, a high amount of noise, and little information stored in the dark image, which has a negative impact on subsequent processing for outdoor computer vision applications. Presently, numerous deep

	learning based methods achieved superior performance with multi-exposure paired training data or additional information. However, obtaining multi-exposure data samples is a tedious task in real-time scenarios. To mitigate this challenge, we propose a zero reference based learnable wavelet approach without multi-exposure paired training data requirement for low-light image enhancement. Our proposed approach generates the low light image and learns to project an image into noise free similar looking image, then we enhance the image using retinex theory. Further, we have proposed learnable wavelet block to remove the hidden noise amplified while enhancement. We introduce Gaussian-based supervision to improve the smoothness of the image. Extensive experimental analysis on synthetic as well as real-world images, along with thorough ablation study demonstrate the effectiveness of our proposed method over the existing state-of-the-art methods for low-light image enhancement. The code is provided at https://github.com/vision-lab-sggsiet/Zero-Reference-based-Low-light-Enhancement-with-Wavelet-Optimization.
13.	Zero waste production technology investigating through gasification process and characterization of its byproducts (Biochar and Bio-Oil) **R Goswami, R Das, S Ganguly** - Proceedings of the 9th International Symposium on Hydrogen Energy, Renewable Energy and Materials, 2023 **Abstract:** This study presents the demonstration of zero waste production technology investigating experimentally by performing the gasification process of eucalyptus biomass and characteristics of its byproducts such as biochar and bio-oil. The outcomes of gasification process in terms of gas composition, calorific value and cold gas efficiency are determined at the optimal operating conditions. The byproducts (biochar and bio-oil) are examined through Gas Chromatography-Mass Spectrometry (GC–MS) and Fourier Transform-Infrared Radiation (FT-IR) spectroscopy in order to find the compounds as well as functional groups respectively. Finally, the uses of gasification products (syngas, biochar and bio-oil) in various fields are emphasized in detail. The experimental outcomes indicated that the calorific value and cold gas efficiency are observed as 5.558 MJ/m3 and 65.68% respectively at the optimal conditions. The bio-oil contains many valuable compounds but Acetic acid is found to be most in percentage (84.93%) among others. The biochar revealed the presence of important functional groups such as alcohol, carboxylic acid, alkyne, isothiocyanate, aromatic compound, sulfoxide and alkene. The gasification products have found a wide application in different sectors to demonstrate the zero-waste production technology.
C	**Journal Article(s)**
14.	A comprehensive review on failure aspects of additive manufacturing components under different loading conditions R Yadav, SS Yadav, **R Dhiman**, R Patel - Journal of Failure Analysis and Prevention, 2024 **Abstract:** Understanding the underlying cause of the failure mechanisms of additive manufacturing (AM) components is essential for developing fatigue-resistant materials and improving the performance of AM components. This comprehensive review article discusses the mechanical failures of AM components including tensile, fatigue, and fracture, which arise due to microstructural heterogeneity influenced by various factors such as porosity, lack of fusion, thermal gradient, powder characteristics, and bonding mechanism. The article also explores the optimization of processing parameters such as beam size, power, temperature, and material deposition rate to enhance resistance against these failures. Additionally, it discusses the various post-processing techniques to mitigate the defects-related issues of additive manufacturing processes, and finally, future research perspectives are pointed out. The comprehensive review contributes to understanding the mechanical and microstructural aspects of the failure mechanisms of the AM components.
15.	A machine learning assisted localization and magnetic field forming for wireless powering of

	biomedical implant devices **VK Srivastava, A Ahmad, A Sharma** - IEEE Transactions on Antennas and Propagation, 2024 **Abstract:** This paper presents an array of overlapped coil transmitter antenna for localizing and generating desired magnetic beams towards the localized receiver to address misalignment problems in near-field wireless power transfer (WPT) applications. For this purpose, a time-divisional approach is employed to obtain the voltage samples from the moving receiver for predicting the position and orientation of the receiver using a machine-learning algorithm. In contrast, particle swarm optimization is utilized to obtain the optimal current distribution to construct a magnetic beam in the receiver direction. The proposed transmitter is also optimized to attain a highly non-uniform magnetic field distribution to improve the localization sensitivity and generate a sharp magnetic beam toward the receiver. The proposed transmitter is fabricated using a high-frequency litz wire and excited using a single source of excitation and switching circuitry. The switching circuitry enables the extraction of voltage samples for localization purposes and constructs the desired magnetic beam. The performance of the fabricated prototype is measured experimentally, which corroborates with analytical results. The results demonstrate the potential of the proposed transmitter to achieve a misalignment-resilient WPT for charging small devices compatible with bio-medical implants, wireless endoscopy capsules, wearable devices, etc.
16.	A mortarboard-shaped receiver antenna for drone wireless charging to achieve an outspread misalignment tolerance towards imperfect landing **S Jain, A Bharadwaj, A Sharma** - IEEE Transactions on Vehicular Technology, 2024 **Abstract:** In drone wireless charging, the performance is highly affected by imperfect landing of drones on the charging pad. To enhance the lateral misalignment tolerance, a novel mortarboard-shaped receiver (Rx) antenna for the drone is proposed. The antenna comprises of five coils and employs a hybrid combining topology integrated with the rectifying circuits to amalgamate the harvested voltages from the individual Rx coils. The design is analytically optimized to efficiently exploit the three orthogonal H-field components generated by the transmitter coil antenna to maximize the Rx misalignment region within which a uniform voltage is received. A low-cost PCB technology is employed to realize the proposed Rx antenna. The analytically optimized design of the proposed antenna is experimentally validated and demonstrates a 90.25% uniformity achieved in the load voltage, which is 276% higher than the conventional Rx coil of the literature. This means that the drone can land anywhere on the ~90% (measured 94%) region of the Tx antenna area without degrading the power transfer performance. The wide tolerance range proves that the proposed Rx can potentially eliminate the lateral misalignment problem to a greater extent for realizing a misalignment tolerant wireless charging system for drones.
17.	A single-phase integrated power charger considering high frequency behaviour for two motor drives fed electric vehicles **A Azeem, AVR Teja, S Payami** - IEEE Journal of Emerging and Selected Topics in Power Electronics, 2024 **Abstract:** This article introduces a fully integrated power charging (IPC) system designed for multi-motor electric vehicles (EVs). The multi-motor drive system, known for its superior acceleration and power capabilities, demands efficient and high-power charging solutions. The high power charging capability is achieved by utilizing both motor and inverter modules as an IPC, which is an inherent feature of multi-motor drive system. In the proposed IPC system both traction inverter and machine winding is utilized without any modification or reconfiguration in the power circuit. The article also delves into the high-frequency behaviour of machine inductance variation during IPC operation, which is critical for understanding winding behaviour at the switching frequency. The proposed system is validated through MATLAB/Simulink and a laboratory prototype across various power levels. Efficiency and power quality are assessed by

	monitoring input power factor and total harmonic distortion, aligning the system with IEEE 519-2022 standards. The proposed system is characterised by notable features, such as the absence of additional hardware requirements and compatibility with a single-phase 230 V, 50-60 Hz power outlet. The results prove the viability and reliability of the proposed IPC operation with the two-motor drivetrain system.
18.	A wearable circulator-like circularly polarised antenna for full-duplex wireless body area network applications **A Thakur, A Sharma**, IJG Zuazola - IET Microwaves, Antennas & Propagation, 2024 **Abstract**: A circulator-like high gain, unidirectional, dual circularly polarised (DCP) wearable antenna with a low specific absorption rate of 0.088 W/kg for 5.8 GHz industrial, scientific, and medical (ISM) band (5.725−5.875 GHz) full-duplex wireless body area network (WBAN) applications is proposed. The DCP full-duplexing is achieved by a closed-loop feedback structure between its orthogonal-ports with enhanced axial ratio (AR) bandwidth and good impedance matching. The antenna is backed with a 7×7 electromagnetic bandgap array that allows for improved directionality, AR and isolation between the ports. The cross-polarisation level above 17 dB is attained in the broadside direction, in both the E-plane and the H-plane, indicating good polarisation discrimination. Since the total power at each respective port is maintained and not halved (−3 dB) with the measured port isolation of ˜28 dB in real scenarios (with the potential evidence of ˜34 dB) within the ISM band, that leads to a circulator-like antenna, meaning that a typically cascaded circulator/duplexer can be relieved and leave to the digital processing any self-interference challenge of full duplex systems through digital cancelation techniques, which alleviates the overall costs of RF hardware and eases integration. Even though dual linear polarization as well as DCP can be supported, the closed-loop feedback structure uses a port as Tx (RHCP) and the other one as Rx (LHCP) simultaneously with enhanced AR bandwidth. Without this structure, it would require a circulator/duplexer for DCP full-duplex operation and the associated added insertion losses and/or 1/2 power (if duplexers) for operation, together with a polarisation misalignment problem that is undesired in wearable WBAN applications.
19.	Adaptive wireless power transfer enabled IoT sensor nodes by a polarization-insensitive scalable planar rectenna module **S Kumar, M Kumar, S Kumar, A Sharma** - IEEE Sensors Journal, 2024 **Abstract:** Wireless power transfer (WPT) has emerged as a promising solution for recharging batteries in low-power IoT sensor nodes. However, implementing WPT-enabled sensor nodes poses a significant challenge due to the requirement of orientation-insensitive operation with a compact footprint and adaptive power requirements. To address these problems, this paper proposes a novel compact polarization-insensitive Rectenna Module (RM) with scalable design feature to achieve adaptive RF power harvesting capabilities. The RM incorporates four sequentially rotated rectenna unit cells (RUCs) to achieve polarization insensitivity. Moreover, RUCs are conjugate matched with the rectifier circuit and their DC outputs are connected in parallel to minimize insertion and combining losses, respectively. The RM offers wider coverage in the broadside direction, with a conversion efficiency of 54.3% at -9.0123 dBm input RF power. The proposed RM has four symmetric DC ports, enabling series and parallel DC combining of multiple RMs to achieve modular scalability. Thus, the polarization-insensitive RM is adaptable to a wide range of user requirements, making it a promising solution for low-power IoT sensor nodes.
20.	Analysis of high temperature and strain amplitude effects on low cycle fatigue behavior of pitting corroded killed E350 BR structural steel **S Chauhan, S Muthulingam, SC Roy** - International Journal of Fatigue, 2024 **Abstract:** High-tension structural steels are prone to accelerated fatigue damage from pitting corrosion and high-temperature. Despite adverse effects, research on their low cycle fatigue

	(LCF) behavior is limited. Specifically, studies analyzing temperature-dependent pit sensitivity effects, considering pit-related material's susceptibility to surface topographic features variation and stress concentration are lacking. This study conducts LCF tests on pitting corroded killed E350 BR structural steel at multiple strain amplitudes and high temperatures. It develops temperature-dependent parameters, such as the cyclic softening pit sensitivity factor, suitable for integration into existing approaches like total cyclic plastic strain energy density (CPSED), power-law, average strain energy density (SED), Coffin-Manson, and pit stress intensity factor (pit-SIF). Further, it proposes multiple linear regression-based prediction models relating total CPSED and average SED with strain amplitude and temperature. Corroded specimens show higher plastic deformation and reduced peak stress, fatigue life, and total CPSED compared to uncorroded ones. The developed parameters, integrated with average SED approach, predicts LCF life within an error band of ±1.5, while power-law relationship reduces it to ±1.2. Moreover, pit-SIF approach estimates fatigue life within an error band of ±1.5. The findings provide critical knowledge for enhanced component design, leading to structural safety, performance, and fire resilience.
21.	AuNP@Self-assembled 4H-Chromene-Enhanced colorimetric detection of Ganciclovir using smartphone Technology: Portable solutions for healthcare G Bhardwaj, R Kaur, S Saini, **N Singh**, N Kaur - Microchemical Journal, 2024 **Abstract:** Any substance, radiation, or radionuclide in our environment that promotes carcinogenesis is a cancerogen. In the current work, we modified the 4H-chromene derivative by covering its surface with a shell of gold nanoparticles. Interestingly, ganciclovir (GCV) formed a bridge between the Nap-group of 4H-chromene and gold nanoparticles to display surface charge reduction properties in AuNP@Self-assembled 4H-Chromene. The surface charge of AuNPs is reduced as a result of the electron transfer mechanism brought on by the creation of the Nap-GCV-AuNP link, which leads to agglomeration. This led to the development of a dual-mode colorimetric sensor for GCV that incorporates solution form and portable sensor strip. The probe showed a linear range of 0–74 nM under ideal circumstances, with a detection limit of 4 nM in solution and 3 nM on paper strip detection. An evaluation of the practical utility in human serum using a portable visual read-out produced satisfactory findings, with a recovery percentage of 102.1 % and a standard deviation of ± 4 %. Surprisingly, this is the first work on the colorimetric detection of Ganciclovir that we are aware of. 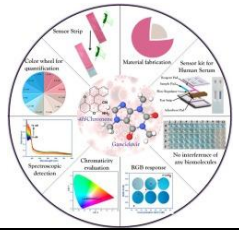
22.	Benzimidazolium salt modified microporous silica-coupled iron oxide nanoparticles: Material engineered for nitrate removal K Gaur, **K Kaur**, G Bhardwaj, N Kaur, **N Singh** - ACS Applied Materials & Interfaces, 2024 **Abstract:** Today's extensive use of inorganic fertilizers in agricultural techniques has increased the concentration of nitrate in drinking water beyond safety limits, causing serious health problems in humans such as thyroidism and methemoglobinemia. Therefore, the present work describes the synthesis of a benzimidazolium salt-based fluorescent chemosensor (KG3) via a multistep synthesis which detects nitrate ions in aqueous medium. This was validated using various analytical techniques such as fluorescence spectroscopy, UV–visible spectroscopy, and electrochemical studies with a detection limit of 0.032 μM without any interference from other active water pollutants. Subsequently, KG3 is further modified with the help of iron oxide nanoparticles (Fe_3O_4 NPs) and silica to obtain the SiO_2@Fe_3O_4-KG3 nanocomposite, which was

	immobilized over a polyether sulfone membrane and evaluated for removal of nitrate ions from groundwater with a removal efficiency of 96%. Moreover, the engineered composite membrane can serve as a solid-state fluorescence sensor to detect NO_3^- ions, which was demonstrated through a portable mobile-based prototype employing a hue, saturation, and value parameter model.
23.	BLE periodic advertising based energy efficient sensor node operation for transfer of large data in monitoring applications **S Gautam, S Kumar** - IEEE Internet of Things Journal, 2024 **Abstract:** IoT applications like livestock and personalised health care monitoring systems have large amounts of data obtained per second from sensors interfaced to battery operated sensor nodes. In such networks, all the data generated at the nodes must be successfully sent to the central receiving device ensuring minimal power consumption of the data transmission operation, to enable longer lifetimes of battery-operated sensor nodes. In this paper, in order to minimize energy consumption of sensor nodes, we propose a Bluetooth Low Energy (BLE) based data transfer approach relying on BLE periodic advertisements, which allow up to 255 bytes of payload to be sent in one packet and minimize the involvement of interference prone primary advertising channels in the data transfer process. By using primary channel transmissions only for one-time device discovery and then disabling them, the proposed technique ensures that number of transmissions made by each sensor node for successful data delivery in large sensor networks is reduced in comparison with conventional extended and periodic advertisements. This offers reduction in energy consumption of sensor nodes due to reduction in radio on time. Through extensive real-time and simulation-based experimentation conducted, we have shown that, in a network of 200 sensor nodes, the proposed periodic advertising based technique requires much lesser radio on time for reliable data delivery and reduces energy consumption of the sensor nodes by almost 51% and 20% as compared to the consumption when extended and standardized periodic advertisements are used to communicate the data, respectively.
24.	Cancer pharmacoinformatics: Databases and analytical tools P Kamble, PR Nagar, KA Bhakhar, P Garg, ME Sobhia, **S Naidu**, PV Bharatam - Functional & Integrative Genomics, 2024 **Abstract:** Cancer is a subject of extensive investigation, and the utilization of omics technology has resulted in the generation of substantial volumes of big data in cancer research. Numerous databases are being developed to manage and organize this data effectively. These databases encompass various domains such as genomics, transcriptomics, proteomics, metabolomics, immunology, and drug discovery. The application of computational tools into various core components of pharmaceutical sciences constitutes "Pharmacoinformatics", an emerging paradigm in rational drug discovery. The three major features of pharmacoinformatics include (i) Structure modelling of putative drugs and targets, (ii) Compilation of databases and analysis using statistical approaches, and (iii) Employing artificial intelligence/machine learning algorithms for the discovery of novel therapeutic molecules. The development, updating, and analysis of databases using statistical approaches play a pivotal role in pharmacoinformatics. Multiple software tools are associated with oncoinformatics research. This review catalogs the databases and computational tools related to cancer drug discovery and highlights their potential implications in the pharmacoinformatics of cancer.
25.	Charge transfer mediated photoluminescence engineering in WS_2 monolayers for optoelectronic application B Luhar, **R Dhankhar, RV Nair**… - ACS Applied Nano Materials, 2024 **Abstract:** Optical emissions from two-dimensional transition metal dichalcogenides greatly differ from sample to sample due to their interactions with different substrates with variations in parameters such as the dielectric constant, absorption coefficient, growth conditions, strain, and

	defects. Often, the mechanisms of environmentally sensitive optical emission in 2D materials are lacking, and it is essential to perform the measurements on the same sample with different substrate backgrounds, which is a challenge. In this work, we explore photoluminescence engineering by comparing the optical properties of WS_2 on SiO_2, TiO_x, and Pt by selectively creating different environments locally on the same sample. The PL-confocal map with good spatial resolution reveals that the emission of WS_2 on TiO_x and Pt is suppressed by charge transfer at the interface. While moving from WS_2 on Pt toward WS_2 on the TiO_x region, a 3-fold enhancement in PL emission has been observed in agreement with a 20% increase in the trion-to-exciton ratio and calculated carrier densities. Further, the transient absorption spectroscopy shows faster exciton recombination in WS_2/Pt (~5.7 ps) and WS_2/TiO_x (~7.2 ps) than WS_2/SiO_2 (~48.5 ps), confirming the charge transfer in varied optical emission of the WS_2 monolayer. Our method paves the way for using charge transfer and controlled carrier injection to design nanoantennas, optoelectronic devices, and quantum optical cavities in 2D materials.
26.	Comparative analysis of entropy generation in smooth and micro-fin tubes using R513A refrigerant: A parametric study NK Vidhyarthi, **S Deb**, S Pal, AK Das - International Journal of Refrigeration, 2024 **Abstract:** Currently, although significant advancements have been made in understanding heat transfer coefficients and pressure decreases in different tube shapes, there is still a noticeable lack of detailed studies on the generation of entropy under flow boiling conditions. In this work, the entropy generation in micro-fin tubes (MFT1 and MFT2) and smooth tubes (ST1 and ST2) in flow boiling conditions experimentally investigated with refrigerant R513A. Research focused on evaluating influence of different input parameters on entropy generation, specifically contribution of heat transfer coefficient (HTC) and total pressure drop (TPD) on entropy generation for all testing tubes. As at a heat flux of 6 $kW \cdot m^{-2}$ and a saturation temperature of 12 °C, MFT1 shows HTC contributions to entropy generation ranging from 0.032 to 0.156 $W \cdot K^{-1}$, while MFT2 ranges from 0.03 to 0.14 $W \cdot K^{-1}$. TPD contributions for both MFT1 and MFT2 range from 0.001 to 0.04 $W \cdot K^{-1}$. Hence, MFT2 shows better results than MFT1 as low entropy generation required for a good heat exchanger. Among input parameters, heat flux displays the highest sensitivity, indicating its significant influence on total entropy generation variations, while vapor quality, mass flux, and saturation temperature also demonstrate notable sensitivity. This research helps us design systems that transfer heat more effectively while using less energy. Understanding these factors can lead to more efficient heat exchangers and other thermal systems.
27.	Comparative assessment of process based models for simulating the hydrological response of the Himalayan River Basin **M Kumar, RK Tiwari**, KS Rautela… - Earth Systems and Environment, 2024 **Abstract:** The current study presents a comprehensive assessment of hydrological models, including the Snowmelt Runoff Model (SRM), MIKE HYDRO RIVER NAM model, and Soil and Water Assessment Tool (SWAT), for simulating runoff dynamics in the Beas River Basin (BRB). Utilizing data spanning seven years from 2014 to 2020, the models underwent rigorous calibration and validation processes to evaluate their performance under varying hydrological conditions. The SRM model exhibited commendable performance, with high correlation coefficients (R^2) of 0.85 during calibration and 0.82 during validation, indicating strong agreement between observed and simulated runoff volumes. Similarly, the MIKE HYDRO RIVER NAM model demonstrated satisfactory performance, albeit with a slightly higher root mean square error (RMSE), indicating a reasonable fit between observed and simulated data. In contrast, the SWAT model exhibited relatively lower performance metrics, particularly regarding R^2 and Nash-Sutcliffe Efficiency (NSE) values, suggesting limitations in accurately capturing runoff dynamics, especially during peak flow events. Comparison of model performance highlighted the superior capability of the SRM and MIKE HYDRO RIVER NAM models in

	simulating runoff dynamics, attributed to their robust representation of hydrological processes and comprehensive consideration of relevant parameters. Analysis of water resource management in the BRB emphasized the importance of understanding flow dynamics, particularly seasonal variations in water availability, for effective water resource management. Overall, this study underscores the significance of accurate hydrological modelling for informed decision-making in water resource management and highlights the potential of the SRM and MIKE HYDRO RIVER NAM models for such applications.
28.	Design, synthesis, and antimicrobial activity of biodegradable sodium alginate/COF polymeric films for smart monitoring of food spoilage and active food packaging **A Singh, N Singh**, N Kaur - ACS Food Science & Technology, 2024 **Abstract:** As the human population increases very rapidly, it is necessary to develop an efficient biodegradable packaging material to increase the shelf life of food, guarantee food safety, and reduce spoilage from extreme conditions. To overcome all of these problems, herein, we synthesize smart sensing strips and antimicrobial active food packaging films to prevent molding. For smart sensing of food spoilage, covalent organic frameworks (COFs) were synthesized from 2,4,6-triformylphloroglucinol (TFP) and p-phenylenediamine. Thereafter, COF was incorporated into a sodium alginate polymeric material to obtain sensing strips with highly colorimetric response and augmented mechanical properties. Smart sensing strips were demonstrated on packaged poultry meat. The sensing strips are highly pH-responsive and color changes according to the pH of the surrounding. Sensing responses of COF were also studied for the biogenic amines that evolve during the spoilage of meat using cyclic voltammetry. The SA/COF film was characterized through different techniques including atomic force microscopy, field emission scanning electron microscopy, Brunauer–Emmett–Teller, energy-dispersive X-ray spectroscopy, Fourier transform infrared spectroscopy, and powder X-ray diffraction. In addition to this antimicrobial citral was incorporated into the SA/COF film to prepare an active packaging film, which reduces food spoilage from high humidity, molding, and high-temperature conditions. The active packaging film was applied to the peanuts to avoid mold formation, which increases their shelf life and reduces food wastage. Based on the above research, we designed a polymeric film for smart sensing and packaging of food.
29.	Effect of laser-wire interaction on bead characteristics at non-planar orientations during off-axis directed energy deposition **S Rathor, E Singla, R Kant** - Progress in Additive Manufacturing, 2024 **Abstract:** In the laser-wire directed energy deposition (LWDED) process, the laser-wire interaction (LWI) length directly influences wire melting and the deposition of a uniform layer. However, the effect of LWI length on bead morphology has not been studied due to the lack of a reliable method to calculate LWI length for off-axis wire feed systems. In this work, an analytical model is introduced to predict LWI length at non-planar orientations. The model development considers laser beam diameter, wire thickness, wire feed angles, and substrate tilt angles. It discusses the centre and trailing wire positions on the substrate. Single-bead-on-plate experiments were performed to present the effect of LWI length at non-planar orientations on bead geometry. The experimental findings reveal that the variations in substrate angles and wire feed angles influence bead width, height, and peak shift. The deposited bead geometry was investigated to demonstrate the effect of LWI and laser spot size. This work contributed to investigating the bead geometry at non-planar orientations for the off-axis wire-fed robotic LWDED process. At non-planar orientation, the predicted maximum LWI length was 1.07 mm at a 15° substrate angle and 10° wire feed angle. The melt pool depths were 336 µm, 261 µm, 290 µm, and 183 µm, respectively, with the corresponding laser energy densities of 29 J/mm3, 22 J/mm3, 25 J/mm3, and 16 J/mm3. These findings aid in deciding substrate positions and orientations in additive manufacturing (AM) of thin-walled overhang tubular parts and repair of conformal parts.

30.	Effect of prolonged immersion on corrosion and cavitation resistance of HVOF-sprayed WC-NiCr and WC-Hastelloy cermet coatings **S Halder, G Vinay, A Anupam**…**DK Mahajan, H Singh** - Surface and Coatings Technology, 2024 **Abstract:** This study examines the effects of prolonged immersion in artificial seawater (3.5 wt% NaCl) on the corrosion and cavitation erosion of HVOF-sprayed WC-NiCr and WC-Hastelloy cermet coatings. The investigation simulates the conditions experienced by marine components, like propellers during maintenance shutdowns. X-ray Photoelectron Spectroscopy (XPS) is extensively used to analyse the chemical species on the coating surface as a function of immersion duration, corrosion, and cavitation. The results indicate that WO_3, formed during deposition in WC-Hastelloy coatings, contributes to their poorer fracture toughness and cavitation resistance compared to WC-NiCr coatings. 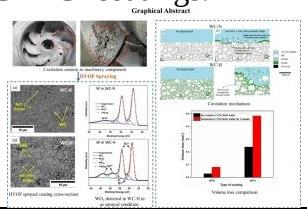
31.	Effect of wire deposition rate on macro and microscopic characteristics of laser weld-brazed AA5083 aluminum alloy to galvanized steel joints and their corrosion response D Narsimhachary, **A Lavakumar**, PK Katiyar, SM Shariff, A Basu - Advances in Materials and Processing Technologies, 2024 **Abstract:** In this study, dissimilar metals, such as aluminium (AA5083) and galvanised interstitial free steel, were laser-brazed in a flange configuration using eutectic filler aluminium wire (4047, Al-12%Si). To investigate the effects of wire deposition rate on the characteristics of laser-brazed joints and to understand the factors contributing to corrosion in these joints. The wire deposition rates were varied while keeping other laser parameters constant. Changes in wire deposition rate were observed to affect the flow behaviour of molten metal leading to variations in the geometrical characteristics of the brazed joints and interfacial reactions as revealed by macroscopic examination. A series of corrosion tests, including electrochemical, immersion, and salt spray tests, were conducted on the laser-brazed joints. It was demonstrated by Immersion corrosion tests that the wire rate influenced the corrosion results for the laser-brazed joints. However, the salt spray test showed no substantial effect on corrosion with respect to different wire deposition rates. Furthermore, the electrochemical results indicated significant changes in the corrosion response of the brazed zone due to the presence of chemically dissimilar phases. A correlative discussion between laser parameters, observed microstructure, and their effects on the corrosion performance of the brazed samples is presented.
32.	Effect of Zn addition on phase evolution in AlCrFeCoNiZn high-entropy alloy **V Shivam**, D Beniwal, Y Shadangi, P Singh… - Advanced Engineering Materials, 2024 **Abstract:** The addition of Zn to AlCrFeCoNi high-entropy alloy (HEA) poses intriguing questions as to how it would affect phase evolution. Herein, the phase evolution in AlCrFeCoNiZn is studied using a combination of experimental techniques (X-ray diffraction, scanning electron microscopy, energy-dispersive spectroscopy, and differential scanning calorimetry) and computational (density-functional theory [DFT], calculation of phase diagrams, and machine-learning) methods. Mechanically alloyed and spark-plasma-sintered AlCrFeCoNiZn assumes a metastable single-phase, body-centered-cubic (BCC) structure that undergoes diffusion-controlled phase separation upon subsequent heat treatment to form separate (Al, Cr)-rich, (Fe, Co)-rich, and (Zn, Ni)-rich phases. The formation of (Al, Cr)-rich phase, not reported previously in AlCrFeCoNi-based HEAs, is attributed to strong clustering tendency of Cr–Zn and

	Cr–Ni pairs, combined with the strong ordering of Zn–Ni pair, driving out Cr that in turn combines with Al to form a (Al, Cr)-rich phase. In the DFT results, the formation of thermodynamically stable $L1_2$ phase is shown wherein Cr–Fe–Zn [Al–Ni-Co] preferably occupy1a (000) [3c (0 ½ ½)] positions. The sluggish diffusional transformation to $L1_2$ phase from BCC precursors is attributed to the small stacking-fault energy of AlCrFeCoNiZn. The equilibrated HEA exhibits a high microhardness of 8.24 GPa with an elastic modulus of 184 GPa.
33.	Electro-photochemical Functionalization of C(sp^3)–H bonds: Synthesis toward Sustainability **P Singh**, B König, **AC Shaikh** - JACS Au, 2024 **Abstract:** Over the past several decades, there has been a surge of interest in harnessing the functionalization of C(sp^3)–H bonds due to their promising applications across various domains. Yet, traditional methodologies have heavily leaned on stoichiometric quantities of costly and often environmentally harmful metal oxidants, posing sustainability challenges for C–H activation chemistry at large. In stark contrast, the emergence of electro-photocatalytic-driven C(sp^3)–H bond activation presents a transformative alternative. This approach offers a viable route for forging carbon–carbon and carbon–heteroatom bonds. It stands out by directly engaging inert C(sp^3)–H bonds, prevalent in organic compounds, without the necessity for prefunctionalization or harsh reaction conditions. Such methodology simplifies the synthesis of intricate organic compounds and facilitates the creation of novel chemical architectures with remarkable efficiency and precision. This review aims to shed light on the notable strides achieved in recent years in the realm of C(sp^3)–H bond functionalization through organic electro-photochemistry. 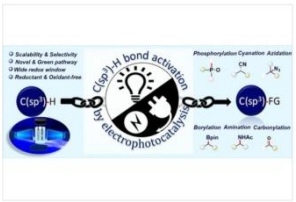
34.	Enhanced corrosion protection performance using polysilazane-derived amorphous SiCN ceramic coating **R Bura, V Girish, RM Prasad** - Surface and Coatings Technology, 2024 **Abstract:** In this work, a polymer-derived silicon carbonitride (SiCN) ceramic layer has been deposited on stainless steel 304 (SS304) to enhance the corrosion resistance of SS304 in a seawater environment. SS304 is dip-coated with a polysilazane solution followed by pyrolysis under argon environment at 800 °C to develop SiCN ceramic layer with a thickness of about 3 μm on SS304. Structural characterization of the prepared samples was performed using Fourier transform infrared (FTIR), X-ray diffraction (XRD), Raman spectroscopy, and scanning electron microscopy (SEM). Potentiodynamic polarization tests of SS304 and SiCN-coated SS304 were performed in 0.6 M NaCl solution. SiCN-coated SS304 showed very low corrosion current density of 4.2×10^{-10} A/cm^2 whereas corrosion current density of uncoated SS304 was measured to be 1.52×10^{-7} A/cm^2. Excellent corrosion resistance performance of SiCN-coated SS304 was observed as confirmed by electrochemical impedance spectroscopic (EIS) measurements.
35.	Fe(iii)-catalyzed p-selective C-H bond chalcogenation of phenols **B Paul, S Ghosh, S Das, I Chatterjee** - Organic & Biomolecular Chemistry, 2024 **Abstract:** An efficient, eco-friendly, and scalable protocol has been introduced for the *p*-selective C–X (X = Se/S) bond formation of phenols employing earth-abundant, less-toxic Fe(III)-catalysts and the green solvent ethanol without using any directing template, stabilizing ligands, oxidants, or additives. The key attraction lies in the impressive *p*-selectivity with moderate to good yields, wide functional group compatibility under mild aerobic reaction conditions, and the synthetic modification of the products towards value-added molecules.

36.	Functionalized covalent triazine framework (CTF) for catalytic CO2 fixation and synthesis of value-added chemicals **R Kishan, P Rani, G Singh, CM Nagaraja** - Crystal Growth & Design, 2024 **Abstract:** The capture and utilization of CO2 for sustainable synthesis of commodity products represent a significant move toward mitigating the growing atmospheric CO2 content for environmental remediation. Meanwhile, Suzuki-Miyaura and Mizoroki-Heck cross-coupling reactions are considerable tools for generating valuable feedstock compounds, such as agrochemicals, natural products, drugs, etc. In this regard, we present the strategic incorporation of catalytically active Pd(II) in a porous covalent triazine framework (CTF) composed of bipyridine sites (bpy-CTF) by postsynthetic modification. Notably, Pd(II) anchored framework, Pd(II)@bpy-CTF, demonstrated exceptional catalytic function in the cyclization of CO2 with propargylic amines and in cross-coupling reactions (Heck and Suzuki-Miyaura), producing high-value commodity products under mild conditions. Further, various electronically and sterically challenging substrates were converted into the corresponding products by using Pd(II)@bpy-CTF as a catalyst. Notably, Pd(II)@bpy-CTF exhibited efficient reusability, sustaining eight catalytic cycles without substantial degradation. The exceptional catalytic behavior of Pd(II)@bpy-CTF is accredited to high abundance of N-rich triazine units and the exposed catalytic Pd(II) sites within the one-dimensional channels of the CTF. This work establishes the potential utility of triazine-based frameworks for utilizing carbon dioxide and stabilizing catalytically active metal ions in developing highly recyclable catalysts to generate value-added chemicals efficiently. 
37.	Gas, temperature & humidity sensors- based onion quality monitoring system **R Raina, KJ Singh, S Kumar** - IEEE Sensors Letters, 2024 **Abstract:** Onions are a valuable cash crop for farmers, providing a reliable source of income, thus monitoring of the quality of onions kept in storage is an important concern. There are various factors like temperature, humidity and storage period that are responsible for maintaining the quality of onion. The common factor is, onion emits various gases when it starts rotting. Thus, to address this issue, carbon dioxide (CO 2), sulphur dioxide (SO 2), hydrogen sulphide (H 2 S), ammonia (NH 3), temperature & humidity (SHT40) sensors are used in the proposed onion quality monitoring system. The paper presents the approximate ranges of the sensors through repeated experiments on three types of onions: healthy, those beginning to rot and fully rotted onions. Additionally, our experiments and the literature both indicate that H 2 S gas is the most effective for early rot detection. Moreover, none of the existing literature works have discussed regarding the power consumption of the onion quality monitoring system. Therefore, a novel battery operated, power efficient onion monitoring device is designed, primarily using H 2 S and SHT40 sensors. This setup has a battery life of approximately 6.03 days with an 11.1 V / 10 Ah battery. When H 2 S levels exceed a threshold indicating the onset of onion rot, all sensors (CO 2 , SO 2 , H 2 S, NH 3 , SHT40) are activated, reducing battery life to 5.41 days.
38.	Generating optical vortex needle beams with a flat diffractive lens **A Kumari, V Dev**, TM Hayward, R Menon, **V Pal** - Journal of Applied Physics, 2024 **Abstract:** We present a novel method for generating optical vortex needle beams (focused optical vortices with extended depth-of-focus) using a compact flat multilevel diffractive lens (MDL). Our experiments demonstrate that the MDL can produce focused optical vortices (FOVs) with topological charges l=1−4 (extendable to other l values), maintaining focus over distances significantly longer than conventional optical vortices. Specifically, FOVs exhibit non-diffracting

	behavior with a depth-of-focus (DOF) extended beyond 5 cm, compared to conventional optical vortices, which show continuous size increase due to diffraction. When the MDL is illuminated by an optical vortex of 3 mm diameter, it achieves a transmission efficiency of approximately 90% and extends the DOF several times beyond that of traditional lenses. Increasing the size of the input optical vortex further extends the DOF but introduces additional rings, with their number increasing proportionally to the value of l. Our approach, validated by both experimental results and numerical simulations, proves effective for beams such as optical vortex and Hermite-Gaussian modes and holds potential applications in high-resolution imaging, material processing, optical coherence tomography, and three-dimensional optical tweezers, offering a simple and efficient solution for generating non-diffracting beams.
39.	High-temperature LCF behaviour of Gaussian-pitted high-strength high-ductility steel rebars **S Chauhan, S Muthulingam** - Engineering Fracture Mechanics, 2024 **Abstract:** Fatigue of high-strength high-ductility steel rebars under pitting corrosion and high-temperature remains largely unknown, specifically concerning temperature-dependent pit sensitivity effects, limiting their widespread adoption despite advantages. This study performs high-temperature, low-cycle fatigue tests on Fe 500D rebars with Gaussian pits. Moreover, experimental results are compared with average strain energy density method, augmented with fractography-based, temperature-dependent parameter models, including exponential pit sensitivity function. Results show accelerated cyclic softening, with up to 94% and 91% reductions in fatigue life and energy dissipation capacity in corroded rebars, respectively. The findings enhance fatigue life predictions, aiding the design of more resilient and safer structures.
40.	How are green stocks and monetary policy related? PK Narayan, **B Garg**, I Gunadi, A Rishanty - Pacific-Basin Finance Journal, 2024 **Abstract:** We propose and test the hypothesis that green stocks and monetary policies are interdependent. Using time-series data for two large economies (India and Indonesia), that have adopted inflation targeting regimes, we develop a structural vector autoregressive model of monetary policy and green stocks that combines with output. We find that green stock prices fall (rise) in response to inflation with a lagged effect and policy rate shocks for India (Indonesia). Currency depreciation, on the other hand, increases green stock prices for India but has a muted effect for Indonesia. We also discover that, for India, monetary policies hardly respond to green stock price shocks while, for Indonesia, green stock prices do influence the evolution of monetary price variables. Our main contribution is that we decipher the effects of green stocks from aggregate market shocks and show each of these market price shocks is related to the monetary aggregates.
41.	Hydrostatic and chemical pressure driven crossover from commensurate to the incommensurate state of the Weyl semimetal $Mn_{3+x}Sn_{1-x}$ K Bhattacharya, AK Bharatwaj, C Singh, **R Gupta**… - Physical Review B, 2024 **Abstract:** The observation of large intrinsic anomalous Hall conductivity (AHC) in the non-collinear antiferromagnetic (AFM) phase of the Weyl semimetal Mn_3Sn generates enormous interest in uncovering the entanglement between the real space magnetic ordering and the momentum space band structure. Previous studies show that changes in the magnetic structure induced by the application of hydrostatic and chemical pressure can significantly affect the AHC of $Mn_{3+x}Sn_{1-x}$ system. Here, we employ the muon spin relaxation/rotation (μ^+SR) technique to systematically investigate the evolution of different magnetic states in the $Mn_{3+x}Sn_{1-x}$ as a function of hydrostatic and chemical pressure. We find two muon sites experimentally, which is also supported by our ab initio calculations. Our μ^+SR experiments affirm that the x = 0.05 compound exhibits a commensurate magnetic state throughout the magnetically ordered phase below the Neel temperature $T_N \approx 420$ K in ambient pressure. In contrast, we observe an incommensurate magnetic state below $T_{IC} \sim 175$ K when a hydrostatic pressure of 1.5 GPa is

	applied. A similar transition from the commensurate to incommensurate state is also found with chemical pressure for x = 0.04 and x = 0.03, using μ^+SR and elastic neutron scattering experiments. Using band structure calculations, we have shown the emergence of Fermi nesting in Mn_3Sn and the subsequent development of incommensurate magnetic ordering under hydrostatic/chemical pressure.
42.	Inelastic scattering of PO^+ by H_2 at interstellar temperatures **P Chahal, A Kushwaha, TJ Dhilip Kumar** - Monthly Notices of the Royal Astronomical Society, 2024 **Abstract:** Phosphorous species are of great interest in interstellar chemistry since they are the basic blocks for building life here on Earth. Modelling the abundance and environment of recently detected PO^+ under non Local Thermodynamic Equilibrium (LTE) requires rotational spectra of the molecule along with accurate collisional rates with the most abundant species, hydrogen and helium. A new 4D *ab initio* potential energy surface (PES) of PO^+ - H_2 collision is calculated using CCSD(T)/CBS(DTQ) methodology considering rigid rotor approximation. The region containing the minima of the PES is augmented using neural networks (NN) model while very high potentials (>2500 cm^{-1}) and asymptotic region have been approximated using Slater and R^{-4} functions respectively. The close coupling calculations have been performed using MOLSCAT software for both *ortho* and *para*-H_2. The rate coefficients have been reported for transitions $\boldsymbol{j - j'} = 1 - 0,\ 2 - 1,\ 3 - 2$ and $5 - 4$ through which PO^+ has been experimentally detected in ISM. The rate coefficients for even and odd transitions of PO^+ with *para*-H_2 are compared with that of helium and are found to be 1.1-2.0 times higher. For even transitions ($\boldsymbol{\Delta j = 2}$), the *ortho*-$H_2$ rates are 10% higher than *para*-H_2 rates. However, the trend reverses in the case of odd transitions ($\boldsymbol{\Delta j = 1}$) when higher *J* transitions are considered at low temperatures. At higher temperatures, the *ortho* rates cross the *para*-H_2 rates and become larger than the latter. The new rate coefficients with both *ortho* and *para*-H_2 will enable accurate modelling of the PO^+ abundance in the interstellar medium under non-LTE conditions.
43.	Influence of dissolved organic matter on U(VI) removal at varying hydrogeochemical scenarios in ultrafiltration process **M Verma, VA Loganathan** - Separation and Purification Technology, 2024 **Abstract:** Uranium (U) is a chemical and radioactive groundwater contaminant that needs to be regulated in drinking water to avoid health hazards. In this study, we have investigated the mechanisms underlying ultrafiltration (UF) process, a low energy-intensive technology, for the removal of uranium from contaminated groundwater, in the presence of dissolved organic matter (i.e. Humic Acid [HA]) under environmentally-relevant conditions representative of regional scenario of Punjab, India. Stirred cell UF experiments with aqueous solutions containing uranium were performed with five different UF membranes with molecular weight cut off (MWCO) ranging from 1 kDa to 30 kDa at a pH of 8.5 that represented ambient groundwater scenario. In the absence of HA, the U(VI) removal was highest for the UF membrane with the lowest MWCO (i.e. 1 kDa) and vice-versa. Further, the effect of various solution parameters viz. pH, concentration of HA, and salinity have been studied using three different UF membranes viz. 5 kDa, 10 kDa, and 30 kDa. Uranium rejection was found to be maximum at pH 5.5 with ca. 97 %, 94 %, and 87 % rejection for 5 kDa, 10 kDa, and 30 kDa membranes, respectively. Further, U(VI) speciation results of the hydrogeochemical model corroborated that the removal of U(VI) in the presence of HA was highly dependent on feed solution pH. Moreover, U(VI) removal increased significantly with an increase in HA concentration, indicating the dominant role of U(VI)-HA complexes. Further, it was observed that increasing the salinity levels to 100 mM in the feed solution (i.e. semi-brackish water scenario) decreased U(VI) rejection primarily due to the charge screening effect. Our results show that using the UF separation process, the World Health Organization's drinking water guideline value of 30 µg of U L^{-1} could be achieved in U(VI) contaminated groundwater that contains significant HA levels.

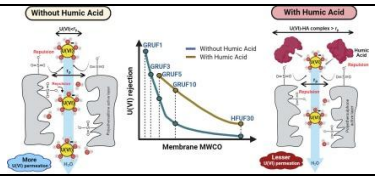

44. [Influence of natural rubber latex thickness on the behavior of jointed rocks during shear wave propagation]
S Rohilla, K Saha, R Sebastian - International Journal of Geomechanics, 2024

Abstract: Understanding the dynamics of rock mass behavior necessitates the study of seismic waves generated by various sources of vibration within rocks. Joints and fractures are prevalent in rock masses and substantially impact their dynamic response to seismic waves. The present study has identified natural rubber latex (NRL) as an effective energy-absorbing medium in the rock masses for limiting wave propagation across the joint. Gypsum plaster has been used to replicate the natural rocks as a model material for conducting this study. The damping properties of rock mass have been determined using split shear plate (SSP) and resonant column (RC) tests. The mechanical response of intact gypsum plaster and NRL has been examined using resonant column testing. The influence of the thickness of the NRL layer on the damping characteristics of the jointed rock mass was studied by varying the thickness of the NRL layer within the joints from 2 to 5 mm. Using RC testing, the variations of shear moduli and damping ratios with different thicknesses of NRL have been studied. The variations of transmission coefficient (T), absorption coefficient (A), and reflection coefficient (R) with variable NRL thickness have been investigated utilizing SSP testing. The findings of the present study can be applied to developing numerical models that can anticipate the behavior of rock masses under dynamic loading conditions and for utilizing the NRL as an effective energy-absorbing material in the rock mass to reduce the vibrations that are transmitted to the structures.

45. [Influences of nanobubbles on particle–particle and bubble–particle interactions: A review]
N Dutta, S Mitra, **N Nirmalkar** - Chemical Engineering Research and Design, 2024

Abstract: The investigation of the interactions between particles resulting from long-range hydrophobic forces has been thoroughly studied in the literature. The hydrophobic force is most likely a result of capillary forces that may occur when nanobubbles merge and create capillary bridges. Recent studies show that fine particle collection can be enhanced by introducing nanobubbles, which seems to be a positive indication of the existence of such capillary bridges. There has been a significant interest in nanobubble research in the past two decades due to their excellent stability and multitude of applications. Although this is an interesting research area, there is still a great debate about the extraordinary stability of nanobubbles. Arguably, much less is known about the underlying mechanisms responsible for their role in bubble–particle and particle–particle interactions that can potentially augment a wide range of separation processes. In this review article, we aim to examine the underlying mechanisms of nanobubble interactions with particles and bubbles that can be conveniently utilized to explain the improved particle separation efficacy. This article also discusses the current understanding of the origin of nanobubbles, including their characterization methods, existing debates, and possible reconciliation of different theories. Finally, the review discusses areas that require further research to clarify some existing issues and provides a direction where further research in the area should be headed.

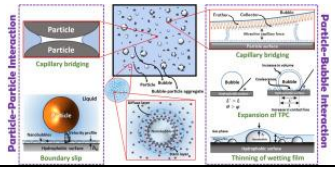

46. [Instability dynamics of viscous fingering interaction on dual displacement fronts]
A Patmonoaji, Y Nagatsu, **M Mishra** - Journal of Fluid Mechanics, 2024

	Abstract: We explored the instability dynamics of the viscous fingering interaction in dual displacement fronts by varying the viscosity configuration. Four regimes of rear-dominated fingering, front-dominated fingering, dual fingering and stable were identified. By using the breakthrough time, which refers to the breakup of the dual displacement fronts, the instability dynamics were modelled, and a regime map was developed. These serve as a tool for effectively harnessing the dual displacement fronts for various applications, such as hydrogeology, petroleum, chemical processes and microfluidics. 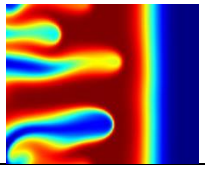
47.	Instantaneous induced braking energy modeling and disperse inverter voltage vector synthesis for maximum energy recovery in IM-based drives **PM Reddy, KR Sekhar** - IEEE Transactions on Industry Applications, 2024 **Abstract:** This paper introduces a novel approach for recovering braking energy in induction motor drives, employing a specific inverter switching sequence. During braking, a phase deviation between the motor voltage and the synthesized inverter voltage is proposed to capture and redirect braking energy back into the DC circuit. To accomplish the phase deviation, in this work, an analytical model for the stator-induced voltage is developed as a function of rotor kinetic energy and magnetic field intensity. Using the developed model, the braking energy recovery characteristics are analyzed by varying the phase deviation (dispersed angles) between the stator-induced voltage and the inverter-synthesized voltage. The investigation by formulating an energy function reveals that the degree of phase deviation significantly impacts energy exchange between the motor and DC circuit during braking. The energy exchange characteristics suggest that energy recovery is possible only when the dispersed angle is more than 180 °; thus, the dispersed angle variation between 180°to 360°is identified as an energy recovery region. The presented work identifies the sector where maximum energy recovery occurs within the energy recovery region. Finally, the analytical findings are validated experimentally by synthesizing various dispersed angles using the inverter, considering the instantaneous motor voltage vector positions as a reference. To recover the extracted braking energy, this work proposes a DC/DC converter-based energy recovery scheme, incorporating monitoring of the DC bus voltage to facilitate energy storage in a battery bank. The proposed method holds promise for enhancing energy utilization efficiency and improving the economic viability of industrial and electric vehicle (EV) drives.
48.	Intervocalic gemination in Mappila Malayalam: Evidence from Perso-Arabic loanwords **PP Raja Thamanna, S Kar** - SKASE Journal of Theoretical Linguistics, 2024 **Abstract:** Gemination, being a common feature of Dravidian languages, has been found to be an effective adaptation strategy in Malayalam (spoken in India). Gemination plays a crucial role in the nativization of loanwords of Perso-Arabic origin (PAO) in the language variety ‘Mappila Malayalam,’ which contains a large number of PAO words. This study attempts to analyze different patterns of gemination in the loanword phonology of the Mappila Malayalam for a range of sounds and their occurrences in various combinations and positions. The field data collected from the northern Malabar region of Kerala (India) indicates a variation in speech with respect to the profound variables, age, geographical region, and education. In progression, the segmental distribution and gemination patterns are phonologically characterized and accounted for within the framework of the stratal optimality theoretic model (Kiparsky 2000). The OT analysis of the PAO words shows certain generalized strategies that can be used to draw implications for syllable structure theories in Malayalam.

49.	Introducing chemoselective peptide conjugation via n-alkylation of pyridyl-alanine: Solution and solid phase applications **S Dutta, A Chowdhury, A Bandyopadhyay** - Organic Letters, 2024 **Abstract:** A novel chemoselective peptide conjugation via late-stage N-alkylation of pyridyl-alanine (PAL) in the solution and solid phase, namely, NAP, is demonstrated. The method constructs functionally diverse and highly stable N-alkylated conjugates with various peptides. Notably, conjugations in the solid phase offered a more economical process. The method can provide the opportunity for dual labeling along with a cysteine handle in a peptide chain. Finally, we showcased that the antiproliferative activities of the p53 peptide (MDM2 inhibitor) could be 2-fold enhanced via NAP conjugation with the RGD peptide (selective integrin binder). 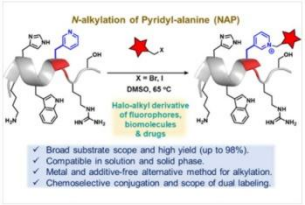
50.	Investigation of radioactivity and heavy metal levels in soil samples from neutral and vegetation land of Punjab, India **SS Kaintura, S Thakur, S Kaur, S Devi, K Tiwari, A Sharma, PP Singh** - Environmental Monitoring and Assessment, 2024 **Abstract:** In this work, radioactivity investigations of soil samples from neutral and agricultural sites in Punjab (India) have been carried out to study the impact of land use patterns. Analyzing soil samples radiological, mineralogical, and physicochemical attributes has employed state-of-the-art techniques. The mean activity concentration of $^{238}U/^{226}Ra$, ^{232}Th, ^{40}K, ^{235}U, and ^{137}Cs, measured using a carbon fiber endcap p-type HPGe detector, in neutral land was observed as 58.03, 83.95, 445.18, 2.83, and 1.16 Bq kg^{-1}, respectively. However, in vegetation land, it was found to be 40.07, 64.68, 596.74, 2.26, and 1.90 Bq kg^{-1}, respectively. In the detailed activity analysis, radium equivalent (Ra_{eq}) radioactivity is in the safe prescribed limit of 370 Bq kg^{-1} for all investigated soil samples. However, the dosimetric investigations revealed that the outdoor absorbed gamma dose rate (96.08 nGy h^{-1}) and consequent annual effective dose rate (0.12 mSv y^{-1}) for neutral land and the gamma dose rate (82.46 nGy h^{-1}) and subsequent annual effective dose rate (0.10 mSv y^{-1}) for vegetation land marginally exceeded the global average. The soil's physicochemical parameters (pH, EC, and porosity) from both sites were measured, and their correlations with radionuclides were analyzed. Various heavy metals of health concern, namely, chromium (Cr), arsenic (As), copper (Cu), cobalt (Co), cadmium (Cd), lead (Pb), mercury (Hg), selenium (Se), and zinc (Zn), were also evaluated in soil samples using Inductively Coupled Plasma-Mass Spectroscopy (ICP-MS). Pollution Load Index (PLI) and Ecological Risk Index (RI) revealed that vegetation land was more anthropogenically contaminated than neutral land, with maximum contamination from Hg and As.
51.	Kerr beam self-cleaning under different initial modal excitation conditions in the anomalous dispersion regime of a graded-index multimode fiber **LK Sharma, V Pal** - Optical Fiber Technology, 2024 **Abstract:** We investigated the phenomenon of Kerr beam self-cleaning (KBSC) under a variety of initial modal excitation conditions in the anomalous dispersion region of a graded-index multimode fiber (GRIN-MMF) by solving the generalized multimode nonlinear Schrodinger equation (GMMNLSE). Our results clearly indicate that the phenomenon of beam self-cleaning is highly dependent on the initial modal excitation conditions, and the power threshold (Pth) required for beam self-cleanup varies depending on the initial modal energy distribution conditions considered. We also show that such beam self-cleanup does not occur for any arbitrary

	initial modal excitation, even at the highest values of input power launched. The temporal and spectral analysis reveals that a spatiotemporal soliton formed initially at a certain power value becomes unstable, thereby shedding dispersive waves and a number of multimode solitons through the fission process, and the nonlinear energy exchanges among the constituent modes lead to a self-cleaned multimode beam. Moreover, we also show that the use of the fiber of longer length permits us to substantially reduce the power threshold (Pth) required to observe beam self-cleaning. Our results realizing the Kerr beam self-cleaning effect with femtosecond pulses in the anomalous dispersion regime of a GRIN-MMF offer innovative and interesting perspectives for the potential extension of the concept of thermalization of classical nonlinear waves to the spatiotemporal domain and may pave the way for a better understanding and control of various novel nonlinear spatiotemporal phenomena in multimode platforms, in developing the next generation of tunable, broadband high-power lasers with nearly single-mode emission.
52.	Laser heat conduction joining of polycarbonate and aluminum alloy **DK Goyal, R Kant** - Proceedings of the Institution of Mechanical Engineers, Part B Journal of Engineering Manufacture, 2024 **Abstract:** The present work demonstrates the laser heat conduction joining (LHCJ) of polycarbonate and aluminum alloy. The experiments are performed to examine the impact of scan speed and laser power on the joint's strength and quality. The bonding between the substrates was assessed by examining the cross-section using a scanning electron microscope and conducting energy-dispersive X-ray spectroscopy. The fractured surfaces are inspected by an optical microscope to explore the bond morphology. A finite-element-based numerical model is developed for the estimation of interface temperature and validated with the experimental results. Results of lap shear tests show that the weld strength is significantly affected by the laser power, scan speed, interface temperature, and bubble area. Microscopic observations of the joint interface disclose bubble area and mechanical interlocking between polycarbonate and aluminum. Through X-ray photoelectron spectroscopy (XPS) analysis, it was discovered that the interface experiences chemical bonding facilitated by the formation of Al-O-C bonds, which effectively enhances the strength of the joint.
53.	LED fluorimetric analysis of Uranium in potable groundwater and associated health concerns RS Negi, M Prasad… **SS Kaintura**… - Journal of Radioanalytical and Nuclear Chemistry, 2024 **Abstract:** The consumption of uranium (U) via drinking water is a health concern due to its potential to pose serious health disorders in the human population. Quantification of U levels in potable groundwater samples (N = 166) from the foothill region of Kumaun Himalaya, India, was done using the LED Fluorimeter to assess associated health hazards. The concentration of U was observed to vary between 0.01 and 26.98 μg L^{-1}. The estimated associated radiological and chemical hazards were observed to pose no considerable health disorders in the human body. The estimated radiation doses were found well below the safe limits. The measured U in groundwater was observed to be strongly correlated with total dissolved solids and electrical conductivity. A comparative analysis of the observed results with other previous studies in northern India is also presented in the paper. The findings of this study will be helpful for future geoscientific studies.
54.	Low power BLE relay node operation in mesh-like architectures for precision agriculture **S Gautam, S Kumar** - IEEE Sensors Journal, 2024 **Abstract:** In this paper, we propose a Bluetooth Low Energy (BLE) based precision agriculture framework, which replaces cluster heads with battery operated relay nodes that relieve the sensor nodes of any extra workload apart from the transmission of their own data, and also help in range extension. The framework imitates BLE mesh, and uses BLE advertisements. Since BLE advertisements provide no inherent synchronization between transmitter and receiver, we propose a novel low power operation for the BLE based relay node in which it learns the schedule of the incoming data packets, and wakes up to scan at certain instants of time when packet reception is

	expected. This helps the relay node to keep scanning disabled and stay in the sleep mode for most of its lifetime. Consequently, the battery lifetime gets prolonged since average current consumption of the scanning operation is just 6 mA, and the sleep current is very small, close to 7.3 μA. We provide power consumption analysis to show the effectiveness of the proposed mechanism in extending the lifetime of the relay node. Further, we found through real time experimentation carried out continuously for 7 days, that with the proposed operation, the relay node is able to achieve on an average 96%, and a maximum of 100% successful reception.
55.	Machining performance of Al3003 alloy during ultrasonic vibration-assisted turning **N Deswal, R Kant** - Journal of the Brazilian Society of Mechanical Sciences and Engineering, 2024 **Abstract:** Ultrasonic vibration-assisted turning (UVAT) is emerged to obtain improved machining performance during the machining process. In this article, experimental work is conducted to analyze machining performance during the conventional turning (CT) and UVAT operations for aluminum 3003 alloy. The microhardness, chip morphology, microstructure, machining temperature, surface roughness, cutting force, tool wear, machined surface damage, corrosion behavior, and residual stresses are analyzed and compared between CT and UVAT. Outcomes revealed that compared to CT, lesser machining force, lesser tool wear, higher temperature, lesser roughness, and lesser surface defects are observed during the UVAT operation. Segmentation, higher thickness, and cracks in chips are obtained for the CT operation whereas negligible chip segmentation, smaller chip thickness, smooth chips, and crack-free chips are observed for the UVAT operation. More grain refinement in microstructure is observed, and higher microhardness is obtained for the UVAT operation compared to the base material (BM) and the CT operation. Compressive residual stresses are attained in UVAT than tensile residual stresses for CT. The corrosion resistance is improved to about 55% in the UVAT operation than the CT operation. The outcomes showed that the machining performance of aluminum alloy is enhanced for UVAT compared with CT.
56.	Microstructural and mechanical properties of Al-5356 alloy structures fabricated using direct energy deposition (DED): In-pursuit to optimizing deposition parameters J Singla, **N Kumar**, A Bansal - Materials Characterization, 2024 **Abstract:** Many industries including aerospace make extensive use of lightweight materials like aluminium alloys because of their extraordinary properties. Wire Arc Additive Manufacturing-Cold Metal Transfer (WAAM-CMT) as a part of modern direct energy deposition technique can be recommended for developing aerospace components of aluminium alloys. However, it is still necessary to investigate the impact of the combined change of developing parameters on some of the crucial qualities including metallurgical and mechanical properties. Therefore, in this part of research work, practically, various process parameters were tried for development of aluminium (Al-5356) alloy walls. Finaly, a specific set of parameters namely wire feed speed, scanning speed and inter layer temperature parameters with two levels of each were selected and with the assistance of these, four walls have been fabricated. Th preliminary analysis showed that low heat input accompanied by higher scanning speed of 60 cm/min and lower wire feed rate of 6 m/min was found to best suitable set of parameters for developing dimensionally stable Al wall with flaw less microstructure. The said set of parameters also showed higher hardness that also accompanied with finer grains, lower percentage towards high angle grain boundary and lower KAM. Even slight variation in these parameters that deal to high heat input can give rise of porosity and misalignment in the wall. Details of microhardness reported high hardness in the bottom part of the wall. However, in a single bead the hardness is higher in the top region, which may be owing to finer grains in the specified region. The above said set of parameters also able to deliver better tensile strength and toughness for Al-5356 alloy. The developed alloy showed improved strength in longitudinal orientation owing to intra layer failure with ductile mode of fracture in contrast to transverse orientation, where the failure mode was reported to mixed

	(ductile as well as brittle) owing to inter layer fracture.
57.	Mott interactions driven insulating behaviour in ruthenium based double perovskites: A_2SmRuO_6 (A = Ba & Sr) **S Dani**, R Pandit, A Babu, **R Kumar** - Journal of Alloys and Compounds, 2024 **Abstract:** Double perovskites (DP's) are important for understanding the diverse physical properties arising from strongly correlated interactions. According to experimental observations, the DP's A_2SmRuO_6 (A = Ba & Sr) are insulators; however, first-principles calculations using GGA approximations show that they are metallic. We observed a band gap (E_g) opening of 1.3 eV for Ba_2SmRuO_6 (BSRO) and 1.4 eV for Sr_2SmRuO_6 (SSRO) upon the insertion of Hubbard parameter (U) in the theoretical computations for accounting the electron-electron interactions. Further investigations using core-level spectroscopy reveal E_g of 1.05 eV for BSRO and 0.85 eV for SSRO. Furthermore, the calculations for Δ (charge transfer energy), U (coulomb repulsion energy), and W (bandwidth) from the combined spectra show U < Δ and U/W > 1.15, which confirms these compounds be classified as Mott-Hubbard insulators. These results expand our understanding of the strongly correlated compounds around the Fermi level, which might have applications in optoelectronics.
58.	Multi-medium image enhancement with attentive deformable transformers **A Kulkarni**, SS Phutke, **SK Vipparthi**, S Murala - IEEE Transactions on Emerging Topics in Computational Intelligence, 2024 **Abstract:** Visibility challenges such as atmospheric haze, water turbidity, etc. are imposed while capturing images in various mediums like aerial, outdoor, underwater, etc. Such reduction in visibility affects the functioning of high-level computer vision applications like object detection, semantic segmentation, military surveillance, earthquake assessment, etc. The existing methods either rely on incorporating additional prior information during the training process or yield less than optimal results when analysed on images with varying levels of degradation, reason being the absence of both local and global dependencies within the extracted features. This paper presents a generalized transformer based architecture for aerial, outdoor and underwater image enhancement. We propose a novel space aware deformable convolution based multi-head self attention containing spatially attentive offset extraction. Here, the deformable multi-head attention is introduced to reconstruct fine level texture in the restored image. Additionally, we introduce a spatially attentive offset extractor within the deformable convolution to prioritize relevant contextual information. Further, we propose an edge enhancing feature fusion block for restoring the edge details in the image along with learning enriched features from multi-stream information. Finally, we propose a global context aware channel attentive feature propagator having a dual functionality of global information extraction and provision of channel attention. Comprehensive experimentation conducted on both synthetic and real-world datasets, along with thorough ablation study, showcases that the proposed approach performs optimally when compared with the existing methods on aerial, outdoor, and underwater image enhancement.
59.	Nanohydroxyapatite-loaded, self-assembled peptide gels for antibacterial and osteogenic activities **P Bundel, V Chawla, AJ Saikia, Y Singh** - ACS Applied Nano Materials, 2024 **Abstract:** Bone constitutes the primary component of the skeletal system, and a substantial reduction in bone density can occur due to trauma, aging, infections, and illnesses. Infections often hinder bone regeneration, with *S. aureus* being the most frequently encountered bacterium in such infections. Peptide-based self-assembled materials have attracted significant interest in the field of biomaterials because of their biomimetic properties, minimal immunogenicity, and ease of production, and peptides, ranging from short to ultrashort length, have been demonstrated to undergo supramolecular self-assembly to form nanofibrous architectures with varying morphology and mechanical strength. Ultrashort peptide gels containing positively charged

	amino acids have demonstrated potent antibacterial properties and possess the ability to mimic the extracellular matrix (ECM). Peptide-based bone regeneration scaffolds incorporating antibiotics have been investigated over the years, but they suffer from erratic antibiotic release from scaffolds and the development of antimicrobial resistance in bacteria. Inspired by the natural ECM of bone, where nanohydroxyapatite (HAp) crystals adhere to collagen fibers and provide strength and support for the growth and differentiation of bone cells, we have developed nanofibrous hydroxyapatite-loaded antibacterial tripeptide gels having osteogenic differentiation potential. The nanofibrous peptide gels entrapping HAp nanoparticles were visualized using FE-SEM and AFM. The gels showed good viscoelastic properties, with mechanical strengths in the range of 1.3 to 12.3 kPa and showed potent antibacterial activity (>85%) against *S. aureus*. The gels were cytocompatible and supported the growth, migration, and differentiation of osteoblast precursor MC3T3-E1 cells. This antibiotic-/growth factor-free approach addresses the constraints associated with the conventional antibacterial bone regeneration scaffolds while showing excellent osteogenic and antibacterial activities. The antibacterial peptide gels reported in this work show promise as bionanomaterial-based bone regeneration scaffolds for treating infected bone defects. 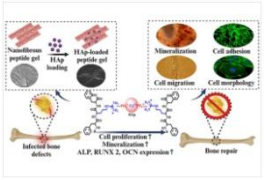
60.	Novel Mn and Si alloyed complex phase steel for automotive applications **S Chand**, S Reza, K Biswas, **RM Prasad, K Rakha** - Materials Science and Engineering: A, 2024 **Abstract:** Automotive industries require materials with higher strength, plasticity and crashworthiness, aiming for 3rd generation of advanced high strength steels (AHSS) with medium Mn, Si and minor alloying elements. In this investigation, 3rd generation AHSS were synthesized using a vacuum arc melting furnace with manganese (Mn) and silicon (Si) as major alloying elements as well as minor additions such as Cr, Al, Ni, etc. The steels thus developed were characterized using FE-SEM, XRD, microhardness tester, universal testing machine (UTM) and 3-dimensional Atom Probe Tomography (APT). The alloy steels after casting and homogenization were subjected to hot rolling at 1100 °C, with rolling exit temperature 900 ± 50 °C. The FE-SEM micrographs in SE mode revealed a complex phase microstructure with martensite, ferrite, bainitic ferrite and retained austenite in the specimens obtained after rolling and air cooling. The microhardness of the developed alloys is found in the range of 395–502 VHN in the hot-rolled and air cooled condition of the specimen. The tensile strength of alloys was measured to be in the range of 1412–1614 MPa with elongation of 12.12 %–18.92 %. The analysis of fracture surfaces after tensile tests for developed alloys revealed that Alloy 1 (Fe-4Mn-1.5Si) had dimples indicating ductile fracture while Alloy 2 (Fe-6Mn-1.5Si) has a mixture of dimples and facets, and Alloy 3 (Fe-8Mn-1.5Si) has lower dimples but larger facets, confirming quasi-ductile fracture with a lower ductility limit of 12.12 %. Atom Probe Tomography was performed to study the complex phase structure at nanoscale through re-distribution of carbon and other alloying elements. 3D APT revealed the presence of very fine retained austenite film of thickness ~4–5 nm and carbon content of 6–8 at.%. This complex phase microstructure obtained after hot rolling and normalizing is made of very fine bainitic ferrite with film type retained austenite providing TRIP effect, in addition martensite and ferrite resulting in high strength.
61.	Nucleophilic ring opening of donor–acceptor cyclopropanes through umpolung reactivity of organochlorophosphines: Phosphine oxide-functionalized boron-pendanted compounds **B Gopal, M Lamba, A Kushwaha, PR Singh, TJ Dhilip Kumar, A Goswami** - Organic Letters, 2024

	Abstract: We present a novel set of frustrated Lewis pair (FLP) systems that exhibit a remarkable ability to promote the ring opening of donor–acceptor cyclopropanes (DACs). This FLP-promoted protocol offers umpolung reactivity of R^1R^2PCl/CN (R^1, R^2 = aryl, alkyl) toward DACs via nucleophilic ring-opening reactions to provide phosphinated boron-pendanted diester compounds. This novel approach exhibits the dual role of $BF_3{\cdot}OEt_2$ as an activator and a reactant. The resulting compounds were found in both the keto and enol forms, with the majority being in the keto form, according to NMR analysis. The enol form was identified by single-crystal XRD analysis, and DFT calculations indicated that the keto form is more stable than the corresponding enol form. 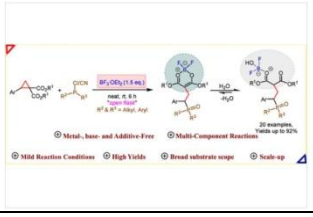
62.	On meromorphic harmonic functions with a pole at the origin **J Parashar, A Sairam Kaliraj** - Complex Analysis and its Synergies, 2024 **Abstract:** In this article, we investigate meromorphic univalent harmonic functions having a simple pole at the origin. First we establish sufficient conditions for the univalence of function *f* within the broader class of meromorphic harmonic functions. Then, we derive coefficient estimate for some geometric subclasses of meromorphic univalent harmonic functions. Subsequently, we provide several necessary and sufficient conditions for *f* to be hereditarily λ-spirallike. Finally, we offer a comprehensive characterization of hereditarily meromorphic harmonic Archimedean and hyperbolic spirallike functions.
63.	On odd univalent harmonic mappings **K Jaglan, A Sairam Kaliraj** - Analysis and Mathematical Physics, 2024 **Abstract:** Odd univalent analytic functions played an instrumental role in the proof of the celebrated Bieberbach conjecture. In this article, we explore odd univalent harmonic mappings, focusing on coefficient estimates, growth and distortion theorems. Motivated by the unresolved harmonic analogue of the Bieberbach conjecture, we investigate specific subclasses of S^0_H, the class of sense-preserving univalent harmonic functions. We provide sharp coefficient bounds for functions exhibiting convexity in one direction and extend our findings to a more generalized class including the major geometric subclasses of S^0_H. Additionally, we analyze the inclusion of these functions in Hardy spaces and broaden the range of *p* for which they belong. In particular, the results of this article enhance understanding and highlight analogous growth patterns between odd univalent harmonic functions and the harmonic Bieberbach conjecture. We conclude the article with 2 conjectures and possible scope for further study as well.
64.	Oxidative cleavage of α-O-4, β-O-4, and 4-O-5 linkages in lignin model compounds over P, N Co-Doped Carbon Catalyst: A metal-free approach **A Chauhan, D Rajendra Kanchan, A Banerjee, R Srivastava** - ChemSusChem, 2024 **Abstract:** Developing efficient metal-free catalysts for lignin valorization is essential but challenging. In this study, a cost-effective strategy is employed to synthesize a P, N co-doped carbon catalyst through hydrothermal and carbonization processes. This catalyst effectively cleaved α-O-4, β-O-4, and 4-O-5 lignin linkages, as demonstrated with model compounds. Various catalysts were prepared at different carbonization temperatures and thoroughly characterized using techniques such as XRD, RAMAN, FTIR, XPS, NH_3-TPD, and HRTEM. Attributed to higher acidity, the P_5NC-500 catalyst exhibited the best catalytic activity, employing H_2O_2 as the oxidant in water. Additionally, this metal-free technique efficiently

converted simulated lignin bio-oil, containing all three linkages, into valuable monomers. Density Functional Theory calculations provided insight into the reaction mechanism, suggesting substrate and oxidant activation by P−O−H sites in the P_5NC-500, and by N−C−O−H in the CN catalyst. Moreover, the catalyst′s recyclability and water utilization enhance its environmental compatibility, offering a highly sustainable approach to lignin valorization with potential applications in various industries.

65.

Perfect Italian domination on some generalizations of cographs

K Paul, A Pandey - Computational and Applied Mathematics, 2024

Abstract: Given a graph G=(V,E), the Perfect Italian domination function is a mapping f:V→{0,1,2} such that for any vertex v∈V with $f(v)$ equals zero, $\sum_{u\in N(v)} f(u)$ must be two. In simpler terms, for each vertex v labeled zero, one of the following conditions must be satisfied: (1) exactly two neighbours of v are labeled 1, and every other neighbour of v is labeled zero, (2) exactly one neighbour of v is labeled 2, and every other neighbour of v is labeled zero. The weight of the function f is calculated as the sum of $f(u)$ over all u∈V. The Perfect Italian domination problem involves finding a Perfect Italian domination function that minimizes the weight. We have devised a linear-time algorithm to solve this problem for P_4-sparse graphs, which represent well-established generalization of cographs. Furthermore, we have proved that the problem is efficiently solvable for distance-hereditary graphs. We have also shown that the decision version of the problem is NP-complete for 5-regular graphs and comb convex bipartite graphs.

66.

Performance analysis of sub-cooled transcritical CO2 refrigeration system using vapour absorption refrigeration system and dew point evaporative cooling

R Beniwal, H Tyagi - Energy, 2024

Abstract: Shifting towards natural refrigerants is expected to reduce the environmental damage in terms of refrigerants leaks, as they have zero ozone depletion potential as well as minimal global warming potential. A CO2 transcritical cycle is analysed thermodynamically in this study. Further, to improve the performance of the CO2 system, a vapour absorption refrigeration system (driven by the heat available at the exit of the compressor) has been integrated with it. Also, to counter the effects of hot climatic conditions, in Indian context, a dew point evaporative cooling system is further utilized to take up the heat from the gas-cooler. A thermodynamic and economic study of the proposed integrated system is performed. The effect of various performance parameters; such as ambient dry bulb temperature, relative humidity, evaporator temperature has been studied on the overall performance of the system. Compared to the base case, the coefficient of performance is improved in the range of 40%–270 %, for the hybrid systems, under the different climatic conditions. Moreover, the proposed system provided a low-cost performance of about 0.024 $/kWh, as compared to the base case consumption of about 0.05 $/kWh.

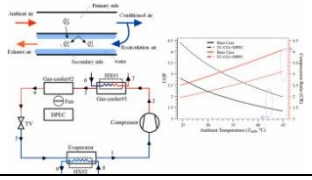

67.

Plasmonic coupling effect of annealed gold nanoarrays

GP Singh, B Fuhrmann, F Syrowatka, J Schilling, **N Sardana** - Physica Scripta, 2024

Abstract: Periodic metal nanodisc arrays have the potential to exhibit regularly spaced large local field enhancements, especially when high-Q collective plasmonic grating resonances can be obtained. Here we demonstrate how Laser interference lithography (LIL) as a maskless and high throughput technique can be used to fabricate these on square centimeter areas. The drawback of LIL is the rather fixed ratio of the size of the individual nanostructure (d) to the period of the

	array (p) of about d/p ~ 0.5 for the setup used in the current article, thereby, limiting its ability to create resonances with ultra-high quality factors (Q-factors). To improve the Q-factor of the resonances of the arrays, we study the effect of thermal annealing nanodisk arrays fabricated by LIL and a lift off process. The nanodisk arrays with periods of 400 nm and 500 nm exhibited a plasmonic resonance, which was caused by the interaction of the single disk resonance and a (1 0) grating resonance. Annealing for a short duration lowered the d/p ratio from 0.5 to 0.4, and led to smoothening of the disk surfaces and growth of gold grains, resulting in lower ohmic and radiative losses and doubling of the Q-factor of the resonances. Finite element method (FEM) simulations were used to monitor this improvement in material parameters. Annealing for a longer duration disintegrated the nanodisk into several smaller particles while maintaining the overall periodicity of the array. While the plasmonic resonances of the experimentally investigated fragmented disks were basically destroyed, simulation predict that for larger periods fragmented nanodisk arrays (keeping the d/p ~ 0.4) can exhibit extremely strong and sharp resonances whose Q-factor increases more than 58.4 times compared to the unfragmented discs. In addition, simulations show a massive enhancement of the local electric field promising immense potential for surface enhanced Raman sensing.
68.	Policy effectiveness in mitigating pandemic-induced macroeconomic impacts: Evidence from large net oil importers of Asia **B Garg** - Emerging Markets Finance and Trade, 2024 **Abstract:** This article employs a two-economy model, which incorporates New Keynesian features, to examine the impact of a coronavirus disease (COVID-19)-induced supply shock on economic recovery in large net oil-importing Asian countries. It examines whether and to what extent monetary and fiscal policies are effective in mitigating such supply shock risks. Our calibrations and estimations reveal that a COVID-19-induced supply shock negatively impacted both the global and domestic economies alike and delayed their economic recovery. Specifically, shocks to total factor productivity and world output negatively affected domestic macroeconomic variables such as domestic output, inflation rate, interest rate, and government expenditure, among others. We show that monetary and fiscal policies efficiently mitigate the adverse effects arising from the supply shock.
69.	Polymer-mediated crack suppression in deposit of nanoellipsoids **D Rani, D Lohani**, MG Basavaraj, DK Satapathy, **S Sarkar** - Langmuir, 2024 **Abstract:** Uniform distribution of particles and crack suppression in dried particulate deposits are major challenges for applications in coating and printing technologies. To address this, we investigated the impact of the addition of a water-soluble polymer, poly(vinyl alcohol) (PVA), on the evaporative self-assembly and kinetics of crack formation in deposits of anisotropic colloids. The fluid flow inside the drying drop is significantly altered due to polymer-mediated adsorption of ellipsoids to the drop surface. The competition between outward capillary flow and Marangoni flow developed in the drying colloid–polymer dispersion drop dictates the distribution of particles in the final dried patterns. The deposits formed by drying drops of ellipsoids dispersed in PVA solutions show three distinct patterns depending on the PVA concentration. A transition from ring-like deposit to uniform deposition with intermittent cracks was observed for a critical PVA concentration of 0.3 wt %. Radial as well as annular cracks were observed in the case of no PVA, while only annular cracks were formed in the dried patterns as the PVA content increased, thus indicating the change of capillary stresses in the films. Analyses of the particle dynamics and deposition patterns confirmed the effectiveness of gelation-driven crack prevention. This method offers a facile and straightforward solution for obtaining crack-free coatings in drying-mediated colloidal nanoparticle assembly.
70.	Probing the electronic ground state of the nitrogen-vacancy center in nanodiamonds at room temperature **R Dhankhar, N Singh, RV Nair** - Optik, 2024

	Abstract: The color centers in diamonds are promising candidates in the context of quantum information science, quantum computation, and spin-based quantum sensors due to their spin-dependent optical transitions. The manipulation and optical readout of electronic spin state is measured using a technique known as optically detected magnetic resonance (ODMR). Here, we discuss the indigenous development of ODMR setup to coherently manipulate and precise readout of spin state of nitrogen-vacancy centers (NV) in nanodiamond at room-temperature. The study involves the confocal mapping of an ensemble of NV centers to measure spin state-dependent optical transition by applying an optical excitation and microwave field simultaneously. The spin state control appears as a dip at 2.87 GHz in the measured emission intensity spectra as a function of microwave frequency. An ODMR contrast of 3.4 % is achieved at the NV center emission maximum of 660 nm and an inhomogeneous dephasing time of 0.03 microseconds. We find an inherent small split in the ODMR dip which is induced by local strain in nanodiamonds. The split becomes stronger while applying an external magnetic field, which forms the basis of NV center-based magnetometry. The results are useful for spin-based microwave-optical quantum transducers, quantum sensing, and quantum memory devices.
71.	Quantum rectification based on room temperature multidirectional nonlinearity in Bi_2Te_3 D Kumar, **R Sharma**, F Wang, Y Liu, S Zhao, H Yang - Nano Letters, 2024 **Abstract:** Recent interest in quantum nonlinearity has spurred the development of rectifiers for harvesting energy from ambient radiofrequency waves. However, these rectifiers face efficiency and bandwidth limitations at room temperature. We address these challenges by exploring Bi_2Te_3, a time-reversal symmetric topological quantum material. Bi_2Te_3 exhibits robust room temperature second-order voltage generation in both the longitudinal and transverse directions. We harness these coexisting nonlinearities to design a multidirectional quantum rectifier that can simultaneously extract energy from various components of an input signal. We demonstrate the efficacy of Bi_2Te_3-based rectifiers across a broad frequency range, spanning from existing Wi-Fi bands (2.45 GHz) to frequencies relevant to next-generation 5G technology (27.4 GHz). Our Bi_2Te_3-based rectifier surpasses previous limitations by achieving a high rectification efficiency and operational frequency, alongside a low operational threshold and broadband functionality. These findings enable practical topological quantum rectifiers for high-frequency electronics and energy conversion, advancing wireless energy harvesting for next-generation communication.
72.	Room-temperature columnar tetragonal self-assemblies based on benzenetricarboxamide and di-ortho substituted azobenzene **A Krishna KM, M Gupta** - ChemPhotoChem, 2024 **Abstract:** Here we report the design, synthesis, and photoresponsive behavior of supramolecular liquid crystalline (LC) materials based on benzenetricarboxamide and di-*ortho* substituted azobenzene. Differential scanning calorimetry, polarized optical microscopy, and wide-angle X-ray scattering studies confirm the formation of columnar tetragonal mesophase at room-temperature. Photoisomerization studies reveal the visible light responsiveness of compounds in solution. Furthermore, we demonstrate supramolecular gel formation, which undergoes irreversible gel-sol transformation upon blue light irradiation, highlighting its potential for light-triggered applications in the field of drug delivery, energy storage etc. 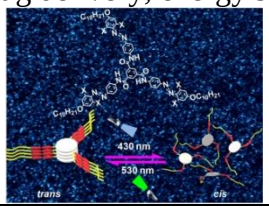
73.	Secondary phase increases the elastic modulus of a cast aluminum-cerium alloy ML Neveau, WR Meier, H Park…**N Bibhanshu**… - Communications Materials, 2024

	Abstract: Alloying in metal castings is one of the principal methods of strengthening an alloy for various structural and functional applications, but very rarely does it modify an alloy's elastic modulus. We report a methodology of combining isostructural Laves phases to form a multi-component, high symmetry, isotropic phase that was discovered to enhance the elastic modulus of a cast aluminum alloy to 91.5 ± 7.4 GPa. Flux grown single crystals of the rhombicuboctahedron phase (RCO), so named for the observed morphology, were used to enhance understanding of the structure and mechanical properties of the phase. The pure RCO phase's structure and site occupancies were co-refined using x-ray and neutron diffraction. Dynamic nanomechanical testing of the cast alloy shows the primary RCO phase has a high, relatively isotropic, elastic modulus. This RCO containing aluminum alloy is found to have a specific modulus that exceeds that of the leading Al, Mg, Steel, and Ti alloys.
74.	SSGAN: Cloud removal in satellite images using spatiospectral generative adversarial network **S Ghildiyal, N Goel**, S Singh, S Lal, R Kawsar, AE Saddik, **M Saini** - European Journal of Agronomy, 2024 **Abstract:** Satellite data's reliability, uniformity, and global scanning capabilities have revolutionized agricultural monitoring and crop management. However, the presence of clouds in satellite images can obscure useful information, rendering them difficult to infer. Aiming at the problem of cloud cover, this study presents a SpatioSpectral Generative Adversarial Network (SSGAN) approach for effectively eliminating cloud cover from multispectral satellite images. It utilizes the Synthetic Aperture Radar (SAR) images as complementary information with the optical images from the Sentinel-2 satellite. The proposed model exploits feature extraction by sub-grouping the 13 channels of Sentinel-2 images based on their electromagnetic wavelength. Experimentally, we demonstrated that the proposed SSGAN model surpasses conventional and state-of-the-art (SOTA) methods and can reconstruct regions obscured by clouds. The subgrouping optimized the utilization of sensor information and improved the performance metrics for reconstructed images. Compared to the state-of-the-art (SOTA) approach, the SSGAN model demonstrates higher performance, achieving a mPSNR of 32.771, mSSIM of 0.880, and correlation coefficient (CC) of 0.889. The SSGAN model was further evaluated under varying conditions, including scenarios without the inclusion of SAR data, where it achieved a mPSNR of 26.825, mSSIM of 0.726, and CC of 0.615. Adding SAR images into the model significantly enhanced its performance, resulting in a mPSNR of 29.932, mSSIM of 0.857, and CC of 0.735. These results indicate that higher mPSNR, mSSIM, and CC values correspond to better image reconstruction quality. Our method enhances the usability of satellite data for crop mapping, crop health monitoring, and crop yield prediction.
75.	Trace principle for Riesz potentials on Herz-type spaces and applications **MA Bhat, G Kosuru** - Journal of Inequalities and Applications, 2024 **Abstract:** We establish trace inequalities for Riesz potentials on Herz-type spaces and examine the optimality of conditions imposed on specific parameters. We also present some applications in the form of Sobolev-type inequalities, including the Gagliardo–Nirenberg–Sobolev inequality and the fractional integration theorem in the Herz space setting. In addition, we obtain a Sobolev embedding theorem for Herz-type Sobolev spaces.
76.	Transcendental nature of *p*-adic digamma values **T Chatterjee, S Garg** - Research in Number Theory, 2024 **Abstract:** For a fixed prime *p*, Murty and Saradha (Acta Arith 133:349–362, 2008) studied the transcendental nature of special values of the *p*-adic digamma function, denoted as $\psi_p(r/p)+\gamma_p$. This research was later extended by Chatterjee and Gun in 2014, who investigated the case of $\psi_p(r/p^n)+\gamma_p$, for any integer $n>1$. In this article, we generalize their results for distinct prime powers and explore the transcendental nature of the *p*-adic digamma values, with at most one

	exception. Further, we investigate the multiplicative independence of cyclotomic numbers satisfying certain conditions. Using this, we prove the transcendental nature of p-adic digamma values corresponding to $\psi_p(r/pq)+\gamma_p$, where p, q are distinct primes.
77.	Transition to a green economy, oil prices and the current account SM Juhro, PK Narayan, **B Garg**, DF Anugrah - Energy Economics, 2024 **Abstract:** In this paper we propose and develop the hypothesis that a transition to a green economy influences the consumption-smoothing component of the current account. This is important because green economy has the potential to improve current accounts. Using a sample of 23 countries, we discover that when renewable energy consumption as a share of total final energy consumption is below the threshold value of 23.561 %, there is a negative impact of oil prices on the current account. However, the negative impact diminishes when renewable consumption exceeds this threshold. Interestingly, splitting the sample into current account surplus and deficit countries reveals that a transition to a greener economy mitigates the negative impacts of an oil price rise more so for deficit countries than surplus countries.
78.	μWSense: A self-sustainable microwave-powered battery-less wireless sensor node for temperature and humidity monitoring **VK Malav, A Sharma** - IEEE Sensors Letters, 2024 **Abstract:** To realise a green IoT sensor network, battery-less wireless sensor nodes (WSNs) are required. This self-sustainability is achieved via energy harvesting from conventional renewable sources such as solar and wind which rely on the weather and are highly expensive. Alternatively, the microwave-based wireless power transfer technique is demonstrated previously, however, only for sensing operations without including the IoT. In this letter, a μ Wave-powered WSN (μ Wsense) hardware is demonstrated to realise true battery-less IoT sensing applications. The μ Wsense consists of a rectenna array (μ wave receiver), power management unit, and BLE module. The μ wave receiver is designed at 5.2GHz to power μ Wsense at a maximum measured transfer range of 2m with a maximum real-time sensing interval of 75 seconds. The minimum harvested power −16.59 dBm is sufficient to operate the μ Wsense.
79.	Vibrational modes of Metribuzin: A theoretical and experimental comparison **G Pal Singh, N Sardana** - ChemistrySelect, 2024 **Abstract:** Pesticides are being used in unregulated and excessive amounts to increase crop yield, causing food and water contamination. Continuous consumption of these pesticides can lead to a variety of health problems, including cancer, respiratory problems, neurological disorders, and reproductive problems. Vibrational spectroscopy uses the unique vibrational modes of these chemicals to identify and quantify their composition with high sensitivity, selectivity, speed, and accuracy. Density functional theory (DFT) can accurately model the vibrational response of these pesticides. Metribuzin, with a triazinone type ring structure, is one such commercial weedicide that is widely used but has not been extensively studied in literature, especially the study of its vibrational modes is lacking. Metribuzin's Raman and infrared (IR) vibrational modes were analyzed in the present article. The calculated bond length, Raman, and IR spectra (using aug-cc-pVTZ B3LYP level of theory) were experimentally confirmed. All the major vibrational modes of Metribuzin were assigned. Also, the basis set comparison was performed for DFT/B3LYP method for Raman spectrum calculation of Metribuzin. The errors in wavenumber and intensity of the Raman vibrational modes for each basis set were compared. Hence, the complete study of Metribuzin's structure and vibrational modes was presented.

	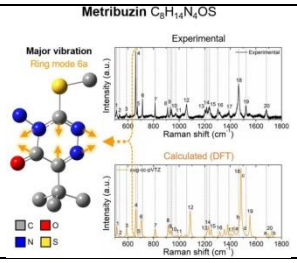

Disclaimer: This publication digest may not contain all the papers published. Library has compiled the publication data as per the alerts received from Scopus and Google Scholar for the affiliation "Indian Institute of Technology Ropar" for the month of September, 2024. The author(s) are requested to share their missing paper(s) details if any, for the inclusion in the next publication digest.